Current Optics and Photonics
Vol. 2, No. 5, October 2018, pp. 482-487

ISSN: 2508-7266(Print) / ISSN: 2508-7274(Online)
DOI: https://doi.org/10.3807/COPP.2018.2.5.482

Theoretical and Numerical Study of Cylindrical-vector-mode Radiation Characteristics in Periodic Metallic Annular Slits and Their Applications

Hyuntai Kim[1] and Yoonchan Jeong[2,3]*

[1]*Optoelectronics Research Centre, University of Southampton, Southampton SO17 1BJ, United Kingdom*
[2]*Laser Engineering and Applications Laboratory, Department of Electrical and Computer Engineering, Seoul National University, Seoul 08826, Korea*
[3]*ISRC & IAP, Seoul National University, Seoul 08826, Korea*

(Received August 10, 2018 : revised August 29, 2018 : accepted August 31, 2018)

We investigate the radiation characteristics of radially polarized light and azimuthally polarized light through plasmonic subwavelength-scale annular slit (PSAS) structures, by means of both theoretical and numerical methods. Effective-medium theory was utilized to analyze the characteristics of PSAS structures, and the corresponding results showed that PSAS structures can function as a metallic medium for azimuthally polarized light, or as a low-loss dielectric medium for radially polarized light. Numerical calculations based on the finite-element method were also performed, to verify the theoretical analyses. It turned out that the numerical results supported the theoretical results. Moreover, we exploited the PSAS structures in novel nanophotonic elements with dual functionalities that could selectively focus or pass/block incident light, depending on its polarization state. For example, if PSAS structures were implemented in the dielectric region of a metallic Fresnel zone plate, the modified zone plate could function as a blocking element to azimuthally polarized light, yet as a focusing element to radially polarized light. On the contrary, if PSAS structures were implemented in the metallic region of a metallic Fresnel zone plate (*i.e.* the inverted form of the former), it could function as a focusing element to azimuthally polarized light, yet as a simple transparent element to radially polarized light.

Keywords : Polarization selection, Effective medium theory, Annular slit, Nanophotonic lens
OCIS codes : (230.5440) Polarization-selective devices; (240.6680) Surface plasmons; (220.3630) Lenses; (050.1380) Binary optics

I. INTRODUCTION

Nanophotonic devices based on various novel structures at subwavelength scales have received a surge of research attention in recent years, as they can offer a lot of fascinating functionalities that conventional optical devices cannot [1-4]. In particular, nanoslits are some of the most investigated nanophotonic structures for extraordinary transmission effects via surface plasmons (SPs), which inherently exhibit strong polarization dependence [1, 5]. In fact, polarization-dependent or -selective nanophotonic structures are favored for a variety of applications, such as display, microscopy, micromachining, biomedicine, etc. [6-9]. Amongst various types of nanoslits, circular slits based on thin metals are an ideal platform for the generation of radially or azimuthally polarized light, *i.e.* a cylindrical vector beam (CVB), which bears the exquisite property of orbital angular momentum, unlike its linearly or circularly polarized counterparts [10]. For example, in micromachining and trapping applications the use of a cylindrical vector beam can offer considerable advantages, from the perspective that it can readily produce even a sub-diffraction-limited hot spot, or a transversely symmetric optical gradient force [7, 11].

In this light, a preliminary experimental study of a novel nanophotonic structure based on plasmonic subwavelength-

*Corresponding author: yoonchan@snu.ac.kr, ORCID 0000-0001-9554-4438
Color versions of one or more of the figures in this paper are available online.

scale annular slits (PSASs) has recently been reported by the authors [5], following the first demonstration of such by Chen *et al*. [12]. This was based on a modified metallic Fresnel zone plate (MFZP) encompassing periodic annular slits at subwavelength scales. Indeed, this study demonstrated that such a nanophotonic structure can offer the novel functionality of polarization-selective supervariable focusing [5]. However, the full characteristics and exploitation of the structure have yet to be investigated in further detail, particularly from theoretical and numerical perspectives. Moreover, a generic approach capable of dealing with such novel annular nanoslits in an analytical manner is essential, because it will play an important role in understanding and justifying their specific functionality.

Therefore, we propose to exploit the effective-medium theory (EMT) [13-15] as a generic theoretical method for analyzing the transmission and reflection characteristics of PSAS structures, for both radially polarized light (RPL) and azimuthally polarized light (APL). We subsequently compare the results from the EMT method to those from a fully numerical approach based on the finite-element method (FEM), verifying the validity of the EMT method under the given conditions. In addition, we also propose and characterize a pair of novel nanophotonic structures that are, in fact, based on the hybridization of MFZP and PSAS structures and have complementary bifocal functionality, depending on the polarization state of incident light.

II. THEORETICAL AND NUMERICAL MODELING

We first define the configuration of the PSAS structure of interest: Based on the preceding experimental demonstration [5], we assume that the substrate and thin metal layer are made of silica and gold respectively. The main design parameters for the PSAS structure are the thickness of the metal layer, the period and duty ratio of the annular slits, and the radius of the innermost annular slit, which determines the initial position of the slit opening. The schematic of the PSAS structure and its specific parameters are illustrated in Fig. 1.

2.1. Theoretical Calculation via Effective-medium Theory (EMT)

Our theoretical approach is based on the EMT [13, 14]. It is worth noting that, while the EMT has previously been used to analyze periodic nanoslits in linear forms [16, 17], it has yet to be exploited for those in circular forms. We think that the EMT is fully applicable to circular nanoslits, because their corresponding eigen-electric fields are invariably parallel or perpendicular to the periodic structures [18]. Thus the EMT can readily provide us with distinct effective indices of a PSAS structure for two of the different eigen-polarization states of incident light, RPL or APL.

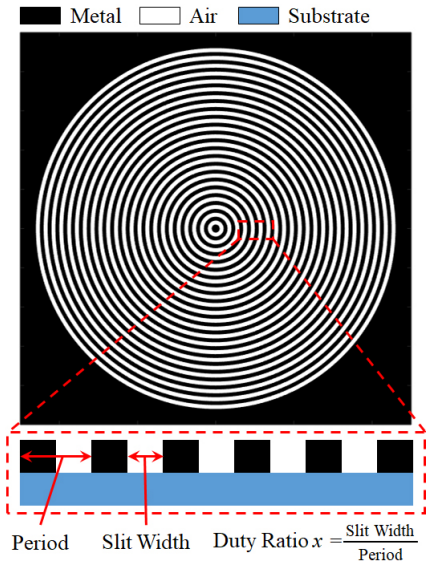

FIG. 1. Schematic diagram of the PSAS structure and its specific parameters.

We note that RPL and APL correspond to the transverse magnetic and transverse electric modes respectively. Without loss of generality, the effective mode indices of the PSAS structure for the two eigen-polarization states are respectively given as the following [13, 14]:

$$n_{eff,r} = \frac{1}{\sqrt{\frac{x}{n_1^2} + \frac{1-x}{n_2^2}}};\ n_{eff,\phi} = \sqrt{x n_1^2 + (1-x) n_2^2}\,, \qquad (1)$$

where $n_{eff,r}$ and $n_{eff,\phi}$ denote the effective mode indices for RPL and APL respectively, and n_1, n_2, and x denote respectively the refractive indices of the two materials that form the periodic annular structure and its duty ratio. In fact, if n_1 and n_2 are justified, which are normally fixed once the materials for the metal layer and its substrate are chosen, then the key parameter that determines the effective indices is the duty ratio of the slit in the radial direction, x. (We note that we have empirically found that if the period was too large ($>\sim$0.3 λ) or the metal layer was too thick ($>\sim$0.6 λ) relative to the wavelength of incident light, the field underwent too much attenuation by Ohmic loss in the metal, regardless of the type of the incident polarization [1, 4], so that the EMT no longer worked effectively, resulting in considerable inaccuracy of the related analysis. Thus we additionally note that such extreme cases are excluded from our current investigation.)

Hereafter, we assume that the wavelength of incident light is 1064 nm, a typical wavelength for a ytterbium-doped fiber laser [10, 19]. Based on Eq. (1), we calculated the effective mode indices of the two eigen-polarization states for three different duty ratios of the periodic annular slits (0.3, 0.5, and 0.7), as summarized in Table 1. For this, we used the material parameters of silica and gold as specified

TABLE 1. Theoretically calculated effective mode indices

Duty ratio (x)	Radial ($n_{eff,r}$)	Azimuthal ($n_{eff,\phi}$)
0.3	1.8682 - 0.0025 i	0.1733 - 5.9985 i
0.5	1.4280 - 0.0008 i	0.1472 - 5.0414 i
0.7	1.2002 - 0.0003 i	0.1156 - 3.8536 i

in [20] and [21], which are $n_{silica} = 1.4496$ and $n_{gold} = 0.20622 - 7.1994i$.

From the real and imaginary parts of the effective mode indices, one can readily deduce that the PSAS structure can function as a "dielectric-like" medium for RPL or a "metal-like" medium for APL. In particular, one can expect that the transmission and reflection of RPL through the PSAS structure will dominantly exhibit oscillatory behavior with respect to the thickness of the metal layer, on account of multiple reflection between the substrate/PSAS and PSAS/air interfaces [22]. In contrast, one can expect that the transmission and reflection of APL through the PSAS structure will dominantly exhibit exponentially decaying and growing behaviors with respect to the thickness. We note that such distinctive behaviors are all due to the fact that the PSAS structure functions as a dielectric-like medium or a metal-like medium, depending on the polarization state of incident light.

Based on the effective mode indices given in Table 1, we theoretically calculated the transmission and reflection characteristics of the PSAS structure for the two different incident polarization states, varying the metal thickness from 40 nm to 600 nm and the duty ratio from 0.3 to 0.7 for a fixed period of 50 nm. We illustrate the results in Fig. 2, where the solid lines denote the results obtained by the EMT method. As expected, one can see that they clearly exhibit oscillatory or exponentially growing/decaying behaviors, depending on the incident polarization state. These trends are in accord with the results demonstrated in previous studies where EMT was exploited to analyze linear periodic nanoslits [16, 17]. In other words, the response of the PSAS structure will be like that of a dielectric film for RPL, or like that of a metallic film for APL.

In fact, in such an effective dielectric or metallic film geometry one can analytically derive the thickness of the film for the resonance t_{res} of RPL or the attenuation length (*i.e.* the penetration depth δ) of APL as $t_{res} = \frac{\lambda}{2Re\{n_{eff,r}\}}$ or $\delta = \frac{\lambda}{4\pi Im\{n_{eff,\phi}\}}$, respectively. Thus, if the optical path length for the round trip of the thin effective medium, $2 \times t_{res}$, is matched to the wavelength of the incident radiation, resonance will occur. In particular, if the real part of the effective mode index is larger than that of the substrate, *i.e.* $n_{eff} > n_{silica}$, then transmission in the forward direction will be maximized. Otherwise, reflection in the backward direction will be maximized.

2.2. Numerical Calculation via the Finite-element Method (FEM)

Building on the theoretical method via the EMT, we have come to know that PSAS structures can offer novel polarization-selective transmission or reflection functionality for CVBs. In this section we further investigate and discuss its detailed characteristics, via a fully numerical method based on the FEM. We note that we utilized a commercial program by COMSOL Multiphysics for the full numerical calculation. All of the simulation parameters were the same as those used with the EMT method, except that a

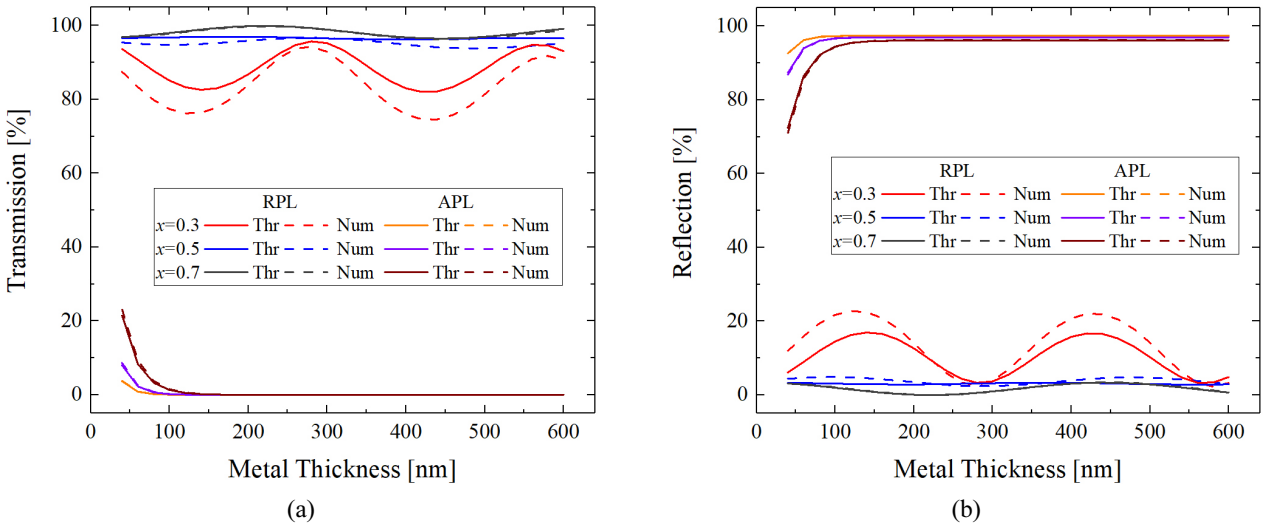

FIG. 2. Transmission and reflection characteristics of the PSAS structure with respect to the thickness of the metal layer and its duty ratio, for RPL and APL. (a) Transmission characteristics obtained by the theoretical (EMT) method (solid lines) and the numerical (FEM) method (dashed lines). (b) Reflection characteristics obtained by the theoretical (EMT) method (solid lines) and the numerical (FEM) method (dashed lines).

first-order Bessel beam with a numerical aperture (NA) of 0.0448 for both RPL and APL was assumed to be incident onto the PSAS structure. We illustrate the full numerical results based on the FEM, in comparison with the theoretical results based on the EMT, in Fig. 2.

From the results, one can see that the theoretical and numerical results are qualitatively in good agreement for both transmission and reflection characteristics, exhibiting the oscillatory behaviors for RPL and exponentially growing/decaying behaviors for APL with respect to the metal thickness, while there are minute quantitative disagreements, to some degree. We note that for $x = 0.5$, the effective mode index of the PSAS structure becomes very similar to the refractive index of the substrate, so that both transmission and reflection responses are negligibly affected by the thickness of the metal layer.

In addition, we calculated the resonance thicknesses and the attenuation lengths, varying the duty ratio of the PSAS structure, where we assumed that the period was fixed at 50 nm. We summarize the corresponding results in Table 2. One can see that both results are also in good agreement.

Building upon the fact that the geometry of the PSAS structure and the incident light both bear cylindrical symmetry, and that its spatial variation is significantly smaller than the wavelength of the incident light, one can justify the validity of EMT for the analysis of the PSAS structure without loss of generality [10, 13]. In fact, we have already shown that the EMT model is applicable to the PSAS structure with reasonably high accuracy in estimating the corresponding transmission rate, decay rate, and resonance thickness, as presented in Fig. 2. However, one can see that there exist some quantitative mismatches of approximately 8% at the most, particularly in the case of $x = 0.3$. This was the case when the metallic portion was significantly larger than the dielectric portion, which was due to the fact that the delicate plasmonic effects became more involved than the approximation by the EMT could handle.

TABLE 2. Resonance thicknesses and attenuation lengths for different duty ratios

Duty ratio (x)	Resonance thickness (t_{res}) [nm]		Attenuation length (δ) [nm]	
	Theoretical	Numerical	Theoretical	Numerical
0.3	284.8	275.8	14.29	14.93
0.5	372.5	278.3	17.21	18.66
0.7	443.3	450	22.62	24.75

III. DISCUSSION

In the preceding section we verified that the EMT method is satisfactorily applicable for analyzing circular nanoslit geometries, *i.e.* PSAS structures. In fact, PSAS structures can efficiently transmit RPL or reflect APL, so that one may consider exploiting PSAS structures for an efficient polarization-selective device, for various applications. For example, implementation of PSAS structures on an optical-fiber facet [23] can offer all-fiberized polarization-selective functionality for various applications in biomedicine, optical trapping, and micro- or nano-machinery [7, 24, 25].

Here we investigate in further detail implementing PSAS structures on an MFZP, which can lead to polarization-selective focusing functionality, as preliminarily demonstrated in [5]. Figure 3(a) shows two examples of a PSAS-implemented MFZP (PSAS-MFZP). In general, a conventional MFZP is designed to have alternating dielectric and metallic regions in the radial direction, following the rule given by the FZP formula [5, 26, 27]. In fact, the metallic regions are covered with metal, whereas the dielectric regions remain uncovered. In contrast, we propose using PSAS structures to replace the dielectric regions or the metallic regions, depending on the purpose of the resultant device. In the first design (see PSAS-MFZP I), the dielectric regions of the MFZP are replaced with concentric PSAS structures. As discussed in the preceding section, one can expect that this device will transmit and focus RPL, but reflect APL. In the second design (see PSAS-MFZP II), the metallic regions are replaced with the concentric PSAS structures.

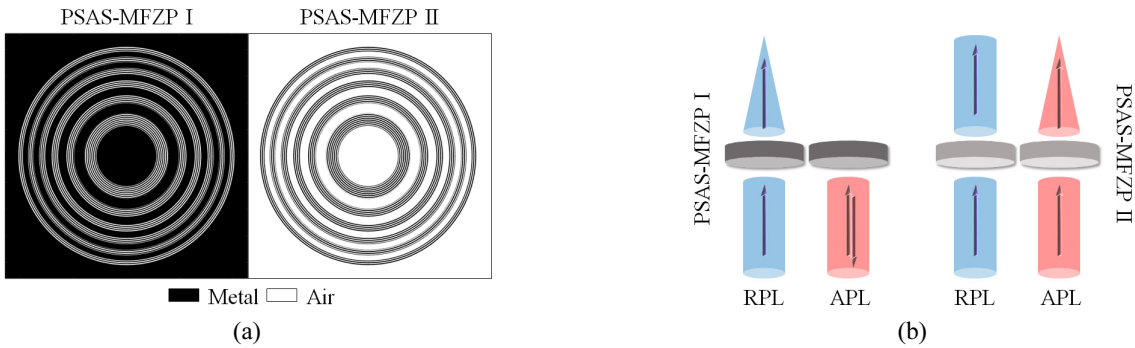

FIG. 3. Two different regimes of polarization-selective functionality by the PSAS-MFZP device. (a) Schematic of two different PSAS-MFZPs. (b) Polarization-selective behaviors of the PSAS-MFZPs.

We stress that this inverted form of the first design is newly proposed here. In this case, the working principle is notably different: For this modified MFZP to work as a focusing element, the light passing through the PSAS sections (originally supposed to be metallic regions) should be blocked. This occurs for APL, because the PSAS structures substantially attenuate the transmission of APL, thereby leading to effective focusing of APL. However, the PSAS structures allow RPL to pass without causing considerable loss, so that the whole MFZP sections will simply transmit RPL. This implies that no focusing occurs for RPL, as depicted in Fig. 3(b).

To verify the characteristics of the two PSAS-MFZPs, we carried out full numerical simulations as follows: We assumed that the duty ratio and period of the PSAS structure in the radial direction were 0.5 and 50 nm respectively, for both designs. For PSAS-MFZP I we set the thickness of the metal layer to 278.3 nm, which in fact showed good transmission and attenuation characteristics for RPL and APL in the preceding section (see Fig. 2). For PSAS-MFZP II we set the thickness of the metal layer to 37.32 nm (*i.e.* $2\times\delta$) to impose a sufficient level of attenuation on APL, as well as to minimize the extraordinary phase evolution in RPL after passing the PSAS sections. We also assumed that the effective focal length of both PSAS-MFZPs was 30 μm. The detailed design parameters of the FZP are summarized in Table 3.

We illustrate the corresponding numerical results in Fig. 4, where one can see the transmission and focusing characteristics of both PSAS-MFZPs for different eigen-polarization inputs, *i.e.* RPL and APL. One can clearly see that both PSAS-MFZPs work exactly as intended. In addition, we note that some minor higher-order focal spots formed at shorter distances were due to the inherent feature of the MFZP, as discussed in [5].

Finally, we would like to compare the transmission rates of the PSAS-MFZPs to those of normal MFZPs having no PSAS structures, particularly when they worked as focusing elements. For PSAS-MFZP I, the PSAS structures were simply removed to form a normal counterpart MFZP that could produce a focal spot equivalently as PSAS-MFZP I. On the contrary, for PSAS-MFZP II the PSAS structures were simply blocked by metal. We carried out numerical simulations of the two normal MFZPs, analyzing their focusing characteristics: They showed that PSAS-MFZP I and PSAS-MFZP II would experience 2.7% and 17.9% reduction in the transmission rates of the focused RPL and APL respectively, relative to those of the normal MFZPs. In the case of PSAS-MFZP I, the reduction rate would be negligibly small; however, in the case of PSAS-MFZP II, the reduction rate would be considerable. This was mainly because the attenuation by the PSAS structures was not high enough to completely eliminate the transmission of APL through the PSAS structures. The attenuation might have been elevated to a sufficient level if the thickness of the metal layer had been further increased. However, we note that increasing the thickness of the metal layer could also lead to a counter-impact on the transmission characteristics of RPL through PSAS-MFZP II. This implies there should be some tradeoff in determining the thickness of the metal layer in PSAS-MFZP II. Notwithstanding, we emphasize that PSAS-MFZP II maintained good focusing functionality for APL even in the current form, as already shown in Fig. 4(d).

TABLE 3. Design parameters of the FZP

Annular-slit order	Inner radius [μm]	Outer radius [μm]
1	5.67	8.06
2	9.92	11.50
3	12.91	14.20
4	15.40	16.54
5	17.61	18.64
6	19.63	20.59

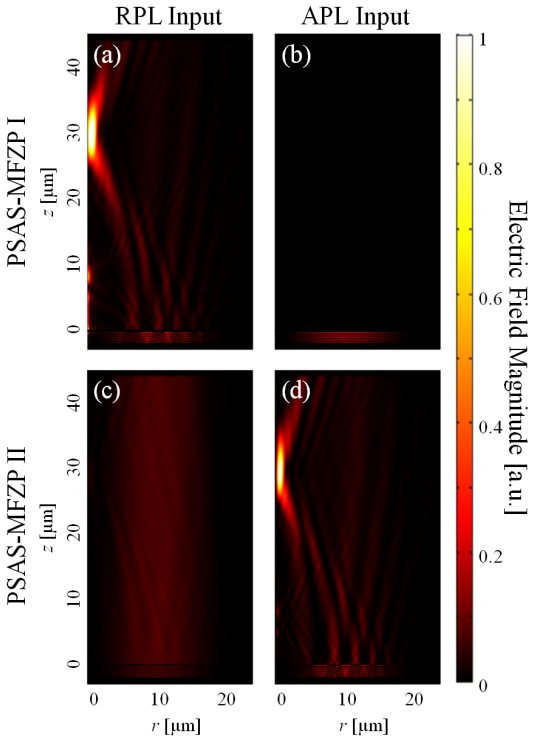

FIG. 4. Electric field pattern of (a) RPL and (b) APL illuminating PSAS-MFZP I. (c) RPL and (d) APL illuminating PSAS-MFZP II.

IV. CONCLUSION

We have carried out a theoretical and numerical study of CVB characteristics in PSAS structures, utilizing the EMT and FEM methods respectively. We verified that the results were in good agreement, unless the period of the

PSAS is too large (> ~0.3 λ) or the metal layer is too thick (> ~0.6 λ) relative to the wavelength of incident light. This was because in such cases the field will be too attenuated by Ohmic loss in the metal, regardless of the incident polarization. We figured out that a PSAS can function as a dielectric material for RPL, or as a metallic material for APL. Moreover, we numerically demonstrated two different types of PSAS-MFZPs by implementing PSAS structures on MFZPs. We showed that PSAS-MFZP I can focus RPL while blocking APL, and that PSAS-MFZP II can focus APL while transmitting RPL. We expect that the proposed PSAS structures can be exploited in various applications that require polarization-selective functionality, for which the EMT method can be useful as a theoretical tool.

ACKNOWLEDGMENT

This study was supported in part by the National Research Foundation of Korea (NRF) grant, funded by the government of Korea (2017R1D1A1B03036201); the Ministry of Trade, Industry and Energy (Project no. 10060150); and the Brain Korea 21 Plus Program.

REFERENCES

1. S. A. Maier, *Plasmonics: fundamentals and applications* (Springer Science & Business Media, 2007).
2. H. Lan and Y. Ding, "Nanoimprint lithography," in *Lithography* (InTech, 2010).
3. R. Liu, T. J. Cui, D. Huang, B. Zhao, and D. R. Smith, "Description and explanation of electromagnetic behaviors in artificial metamaterials based on effective medium theory," Phys. Rev. E **76**, 026606 (2007).
4. H. Kim, H. An, J. Kim, S. Lee, K. Park, S. Lee, S. Hong, L. A. Vazquez-Zuniga, S.-Y. Lee, and B. Lee, "Corrugation-assisted metal-coated angled fiber facet for wavelength-dependent off-axis directional beaming," Opt. Express **25**, 8366-8385 (2017).
5. H. Kim, J. Kim, H. An, Y. Lee, G.-Y. Lee, J. Na, K. Park, S. Lee, S.-Y. Lee, and B. Lee, "Metallic Fresnel zone plate implemented on an optical fiber facet for super-variable focusing of light," Opt. Express **25**, 30290-30303 (2017).
6. S.-W. Ahn, K.-D. Lee, J.-S. Kim, S. H. Kim, J.-D. Park, S.-H. Lee, and P.-W. Yoon, "Fabrication of a 50 nm half-pitch wire grid polarizer using nanoimprint lithography," Nanotechnology **16**, 1874 (2005).
7. K. Venkatakrishnan and B. Tan, "Interconnect microvia drilling with a radially polarized laser beam," J. Micromech. Microeng. **16**, 2603 (2006).
8. Z. Nan, J. Xiaoyu, G. Qiang, H. Yonghong, and M. Hui, "Linear polarization difference imaging and its potential applications," Appl. Opt. **48**, 6734-6739 (2009).
9. K. Aydin, T. Seliga, and V. Balaji, "Remote sensing of hail with a dual linear polarization radar," J. Clim. Appl. Meteorol. **25**, 1475-1484 (1986).
10. H. Kim, Y. Kwon, L. A. Vazquez-Zuniga, S. J. Lee, W. Park, Y. Ham, S. Song, J.-H. Yang, and Y. Jeong, "Rigorous analysis on ring-doped-core fibers for generating cylindrical vector beams," J. Opt. Soc. Korea **18**, 650-656 (2014).
11. Q. Zhan, "Trapping metallic Rayleigh particles with radial polarization," Opt. Express **12**, 3377-3382 (2004).
12. W. Chen, D. C. Abeysinghe, R. L. Nelson, and Q. Zhan, "Plasmonic lens made of multiple concentric metallic rings under radially polarized illumination," Nano Lett. **9**, 4320 (2009).
13. K. Han and C.-H. Chang, "Numerical modeling of sub-wavelength anti-reflective structures for solar module applications," Nanomaterials **4**, 87-128 (2014).
14. Y. Chang, G. Mei, T. Chang, T. Wang, D. Lin, and C. Lee, "Design and fabrication of a nanostructured surface combining antireflective and enhanced-hydrophobic effects," Nanotechnology **18**, 285303 (2007).
15. J. T. Shen, P. B. Catrysse, and S. Fan, "Mechanism for designing metallic metamaterials with a high index of refraction," Phys. Rev. Lett. **94**, 197401 (2005).
16. B. Lee, Y.-B. Chen, and Z. Zhang, "Confinement of infrared radiation to nanometer scales through metallic slit arrays," J. Quant. Spectrosc. Radiat. Transfer **109**, 608-619 (2008).
17. B. Rahmani, A. Bagheri, A. Khavasi, and K. Mehrany, "Effective medium theory for graphene-covered metallic gratings," J. Opt. **18**, 105005 (2016).
18. W. Cai, U. K. Chettiar, A. V. Kildishev, and V. M. Shalaev, "Optical cloaking with metamaterials," Nat. Photon. **1**, 224 (2007).
19. Y. Jeong, J. Sahu, D. Payne, and J. Nilsson, "Ytterbium-doped large-core fiber laser with 1.36 kW continuous-wave output power," Opt. Express **12**, 6088-6092 (2004).
20. I. Malitson, "Interspecimen comparison of the refractive index of fused silica," J. Opt. Soc. Am. **55**, 1205-1209 (1965).
21. D. I. Yakubovsky, A. V. Arsenin, Y. V. Stebunov, D. Y. Fedyanin, and V. S. Volkov, "Optical constants and structural properties of thin gold films," Opt. Express **25**, 25574-25587 (2017).
22. D. K. Cheng, *Field and wave electromagnetics* (Pearson Education India, 1989).
23. W. Chen, W. Han, D. C. Abeysinghe, R. L. Nelson, and Q. Zhan, "Generating cylindrical vector beams with subwave-length concentric metallic gratings fabricated on optical fibers," J. Opt. **13**, 015003 (2010).
24. K. Moh, X.-C. Yuan, J. Bu, S. Zhu, and B. Z. Gao, "Radial polarization induced surface plasmon virtual probe for two-photon fluorescence microscopy," Opt. Lett. **34**, 971-973 (2009).
25. K. C. Neuman and S. M. Block, "Optical trapping," Rev. Sci. Instrum. **75**, 2787-2809 (2004).
26. J. Kim, H. Kim, G.-Y. Lee, J. Kim, B. Lee, and Y. Jeong, "Numerical and experimental study on multi-focal metallic fresnel zone plates designed by the phase selection rule via virtual point sources," Appl. Sci. **8**, 449 (2018).
27. J. Kim, J. Kim, J. Na, and Y. Jeong, "Numerical study of a novel bi-focal metallic fresnel zone plate having shallow depth-of-field characteristics," Curr. Opt. Photon. **2**, 147-152 (2018).